JOURNAL OF GEOPHYSICAL RESEARCH: ATMOSPHERES, VOL. 118, 1247–1260, doi:10.1002/jgrd.50145, 2013

Future change of the global monsoon revealed from 19 CMIP5 models

Pang-chi Hsu,[1] Tim Li,[1] Hiroyuki Murakami,[1,2] and Akio Kitoh[2]

Received 31 July 2012; revised 7 November 2012; accepted 27 December 2012; published 13 February 2013.

[1] The variability of global monsoon area (GMA), global monsoon precipitation (GMP), and global monsoon intensity (GMI) in the present climate (1979–2003) and the future warmer climate (2075–2099) under Representative Concentration Pathways 4.5 (RCP4.5) scenario was examined based on 19 Coupled Model Intercomparison Project Phase 5 (CMIP5) simulations. In the present-day simulations, the ensemble mean precipitation reproduces the observed GMA, GMP, and GMI, although the spread of individual models is large. In the RCP4.5 simulations, most (17 of 19) of the CMIP5 models project enhanced global monsoon activity, with the increases of GMA, GMP, and GMI by 1.9%, 3.2%, and 1.3%, respectively, per 1 K of surface warming. The diagnosis of a column-integrated moisture budget indicates that the increase in GMP is primarily attributed to the increases of moisture convergence and surface evaporation, whereas horizontal moisture advection has little effect. A further separation of dynamic and thermodynamic factors shows that increase of the moisture convergence comes mainly from the increase of water vapor, but is partly offset by the convergence effect. The increase of the surface evaporation is caused by the increase of sea-air specific humidity difference, while the change in surface wind speed plays a minor role. The GMP experiences a great year-to-year variation, and it is significantly negatively correlated with the Niño3.4 index averaged over a typical monsoon year (defined from May to the following April) in the pre-industrial control and present-day simulations, similar to observations. Under the RCP4.5 warming, such rainfall variability is intensified, and the relationship between monsoon and El Niño strengthens. A large proportion of intensification in the year-to-year monsoon rainfall variability arises from the land monsoon region.

Citation: Hsu, P.-c., T. Li, H. Murakami, and A. Kitoh (2013), Future change of the global monsoon revealed from 19 CMIP5 models, *J. Geophys. Res. Atmos.*, *118*, 1247–1260, doi:10.1002/jgrd.50145.

1. Introduction

[2] The monsoon is characterized by a seasonal reversal in lower tropospheric winds and corresponding variations in rainfall amounts [*Webster et al*., 1987] and is the most energetic climate system over the tropics. Billions of people living in global monsoon areas rely on monsoon precipitation for basic human needs, agriculture, and industrial development. Due to the far-reaching impact of monsoon rainfall, simulations and projections of monsoon variability are considered to be an important aspect of climate research [e.g., *Intergovernmental Panel on Climate Change* (*IPCC*), 2007].

[3] Despite large uncertainties in regional rainfall projections [*IPCC*, 2007], a number of signals associated with variations in monsoon rainfall have been identified. Over the South/East Asian monsoon regions, the intensification of summer monsoon rainfall and its interannual variability have been widely detected within model projections [*Hu et al*., 2000; *May*, 2002; *Meehl and Arblaster*, 2003; *Kitoh et al*., 2005; *Ueda et al*., 2006; *Annamalai et al*., 2007; *Lu and Fu*, 2010; *Turner and Annamalai*, 2012]. Based on the Coupled Model Intercomparison Project Phase 3 (CMIP3) multimodel data set, *Moise et al*. [2012] found that the overall Australian summer monsoon precipitation showed little change, but the length of the wet season had increased slightly by the end of 21st century. Considering future changes in the African monsoon system, *Shongwe et al*. [2009] showed that the rainy season over Southern Africa tends to become shorter in a future climate (2051–2200) under the CMIP3 A1B scenario, whereas *Cook and Vizy* [2006] suggested that no consensus has been achieved over the West African monsoon regions. In addition, projected changes in the American monsoon based on the CMIP3 models were diverse [*Giorgi et al*., 2001; *Li et al*., 2006]. Recently, *Hsu and Li* [2012] examined the results of global warming experiments that used an atmospheric general circulation model (AGCM) and the fifth phase of the Coupled Model Intercomparison Project (CMIP5) data set, and noted a projected dipole rainfall anomaly associated with enhanced

[1]International Pacific Research Center, University of Hawai'i at Manoa, Honolulu, Hawaii, USA.
[2]Meteorological Research Institute, Tsukuba, Japan.

Corresponding author: T. Li, International Pacific Research Center, University of Hawai'i at Manoa, 1680 East-West Rd., Honolulu, HI 96822, USA. (timli@hawaii.edu)

2169-897X/13/10.1002/jgrd.50145

rainfall over the Amazon monsoon area and decreased precipitation in the Atlantic intertropical convergence zone (ITCZ) during the austral summer.

[4] Previous modeling studies focused mostly on the variability of monsoon rainfall within a specific monsoon region, as reviewed above. The changes in the global monsoon system as a whole have received less attention. As the annual variation in solar heating is a fundamental driver of monsoon development, *Trenberth et al*. [2000] and *Wang and Ding* [2006] proposed the concept of the global monsoon to describe the strength of overall monsoon systems around the globe. From observations, global monsoon precipitation (GMP) has increased over the past three decades [*Hsu et al*., 2011; *Wang et al*., 2011]. This increasing GMP trend follows the cooling (warming) trend of sea surface temperature (SST) in the eastern Pacific (Indo-Pacific warm pool) [*Wang et al*., 2011]. AGCM experiments [*Zhou et al*., 2008] suggest that the GMP variations arose mainly from ocean forcing, such as the El Niño-Southern Oscillation (ENSO) and Indian Ocean SST anomaly, over the last half-century (1949–2000). The synchronous cycles of GMP and ENSO in 1970–1999 were also captured by the Model for Interdisciplinary Research on Climate (MIROC5) and most CMIP3 coupled models [*Kim et al*., 2011]. However, these studies did not consider the possible changes in global monsoon activity and the linkage between GMP and ENSO in a future warmer climate.

[5] *Hsu et al*. [2012] found that the global monsoon area, precipitation, and intensity all increase from the late 20th century to the late 21st century. The result was primarily based on the simulations of three high-resolution AGCMs. In this study we intend to extend the work of *Hsu et al*. [2012] by analyzing 19 CMIP5 models. Larger samples from the CMIP5 models with different model physics (e.g., different convective parameterizations, air-sea coupling schemes, and Earth's biogeochemical cycles for some Earth System Models) may increase our confidence in the global monsoon projections. The validation of individual CMIP5 models may provide information for model development and improvement in monsoon simulations. Moreover, longer integrations of CMIP5 pre-industrial control runs and global warming experiments can help us understand the interannual variability of global monsoon precipitation and its possible change under a warmer climate, which has not been shown in the previous studies. The overall objective of the current study is to provide a detailed and systematic evaluation of the capability of the CMIP models in simulating global monsoon features, the moisture processes contributing to the GMP changes, and the interannual variability of monsoon rainfall in response to global warming in 19 state-of-the-art coupled GCMs under the World Climate Research Programme's (WCRP) CMIP5 project [*Taylor et al*., 2012].

[6] In the remainder of the paper, section 2 describes the models, observational data, and methodology used in global monsoon analysis. In section 3, we evaluate the capability of the CMIP5 models to reproduce the characteristics of the present-day global monsoon, including the geographical distribution of global monsoon rainy domains, total monsoon precipitation amounts, and the amplitude of global monsoon intensity. Section 4 presents the projected changes in global monsoon activity to the end of the 21st century. The mechanisms responsible for GMP changes are then further examined. Section 5 describes the interannual variability of GMP and ENSO, and their relationship to each other, in both the present-day and a future warmer climate states. The main conclusions of the study are summarized in section 6.

2. Data and Methodology

2.1. CMIP5 Models and Observational Data Sets

[7] Nineteen CMIP5 model outputs (Table 1), from pre-industrial control, historical, and global warming runs, were used to investigate the internal variability of global monsoon

Table 1. The 19 CMIP5 CGCMs Used in This Study

Model	Modeling Center/Group
ACCESS1-0	Commonwealth Scientific and Industrial Research Organization (CSIRO) and Bureau of Meteorology (BOM), Australia
bcc-csm1-1	Beijing Climate Center, China Meteorological Administration
CanESM2	Canadian Centre for Climate Modeling and Analysis
CCSM4	National Center for Atmospheric Research
CSIRO-Mk3-6-0	Commonwealth Scientific and Industrial Research Organization in collaboration with Queensland Climate Change Centre of Excellence
FGOALS-g2	LASG, Institute of Atmospheric Physics, Chinese Academy of Sciences and CESS,Tsinghua University
FGOALS-s2	LASG, Institute of Atmospheric Physics, Chinese Academy of Sciences
GFDL-CM3	NOAA Geophysical Fluid Dynamics Laboratory
GFDL-ESM2G	
GISS-E2-R	NASA Goddard Institute for Space Studies
HadGEM2-ES	Met Office Hadley Centre
INMCM4	Institute for Numerical Mathematics
IPSL-CM5A-MR	Institut Pierre-Simon Laplace
MIROC5	Atmosphere and Ocean Research Institute (The University of Tokyo), National Institute for Environmental Studies, and Japan Agency for Marine-Earth Science and Technology
MIROC-ESM	Japan Agency for Marine-Earth Science and Technology, Atmosphere and Ocean Research Institute (The University of Tokyo), and National Institute for Environmental Studies
MIROC-ESM-CHEM	
MPI-ESM-LR	Max Planck Institute for Meteorology
MRI-CGCM3	Meteorological Research Institute
NorESM1-M	Norwegian Climate Centre

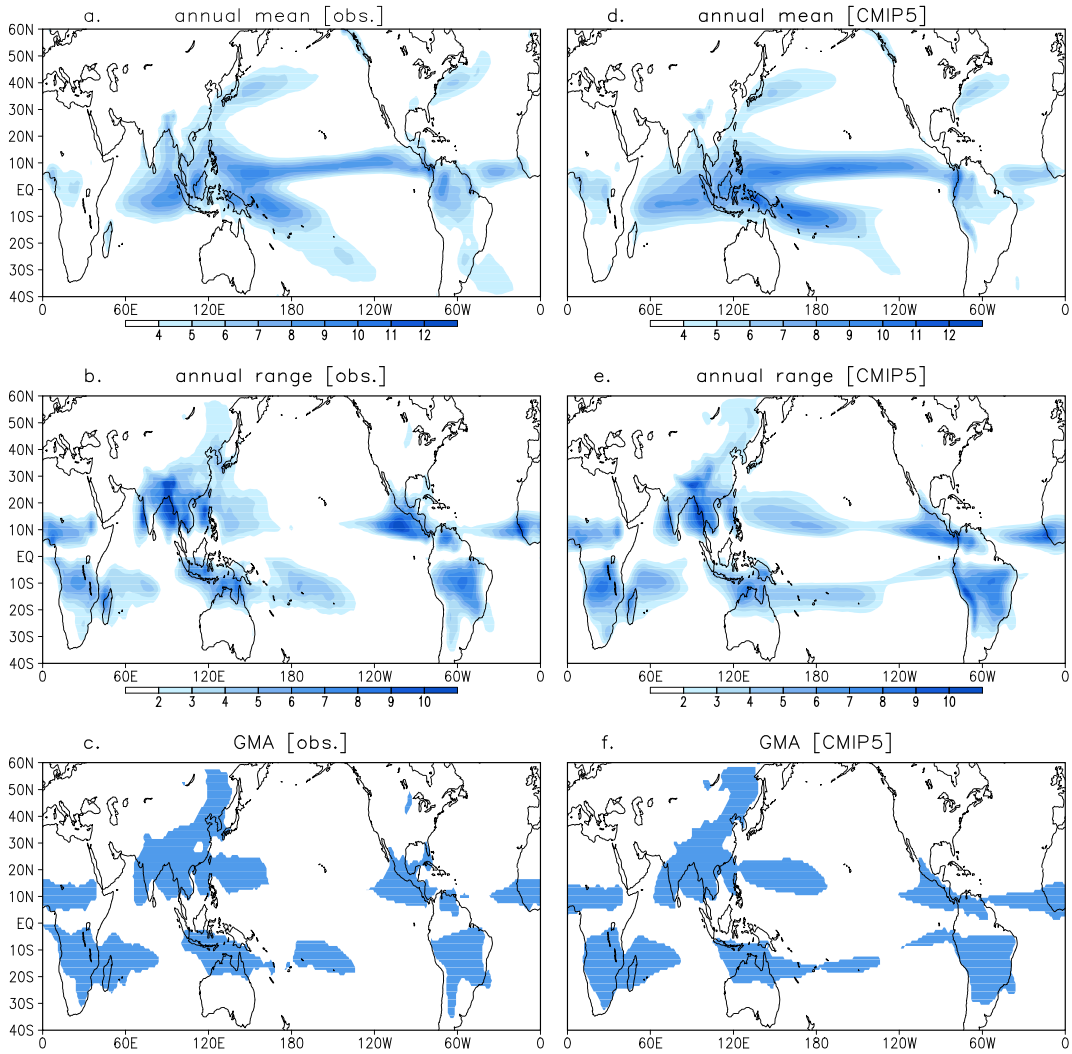

Figure 1. Climatology (1979–2003) of (a) annual mean precipitation (mm d^{-1}), (b) annual range of precipitation (mm d^{-1}), defined as the difference between local summer (JJA in the Northern Hemisphere and DJF in the Southern Hemisphere) and winter precipitation, and (c) GMA derived from the average of GPCP and CMAP rainfall data. (d–f) Same as in Figures 1a– 1c, but based on the MME mean precipitation of the 19 CMIP5 historical simulations.

rainfall and the changes in the global monsoon from the present-day (1979–2003) to a future (2075–2099) climate state, respectively. We chose the Representative Concentration Pathways 4.5 (RCP4.5) experiment, in which the target radiative forcing in 2100 is set to 4.5 W m^{-2}, for the future climate projections, because most models perform simulations based on this scenario. Considering the data available for moisture budget analysis, only one realization from each of the 19 models was analyzed.

[8] Two sets of monthly precipitation data derived from the Global Precipitation Climatology Project (GPCP) [*Adler et al.*, 2003] and the Climate Prediction Center Merged Analysis of Precipitation (CMAP) [*Xie and Arkin*, 1996] were adopted to derive the observed global monsoon features. Since there is some inconsistency in global monsoon rainfall over ocean regions between the GPCP and CMAP data [*Zhou et al.*, 2008; *Hsu et al.*, 2011], an arithmetic mean of the two data sets was used to reduce uncertainty. The horizontal resolution of both the GPCP and CMAP data sets is 2.5° latitude by 2.5° longitude. To more accurately define the monsoon area, the original data sets were interpolated onto a 1° latitude/longitude grid using a bilinear interpolation technique. The same interpolation approach was applied to the CMIP5 models, which have various resolutions ranging from T42 (approximately 2.8°) to T106 (approximately 1.125°), to conduct the multi-model ensemble (MME) analysis. This interpolation does not affect the estimations of global monsoon activity and its change rates. In our sensitivity test, the distributions of monsoon area based on the original model grid and the interpolated grid are quite similar in both the present-day and future climate states. The monsoon change rates derived from the interpolated and non-interpolated grid data are also very close.

[9] The SST data used to evaluate the performance of the models with respect to ENSO amplitude and the relationship between monsoon rainfall and ENSO were obtained from the Hadley Center global sea ice and sea surface temperature data set (HadISST1) [*Rayner et al.*, 2003] and the Extended

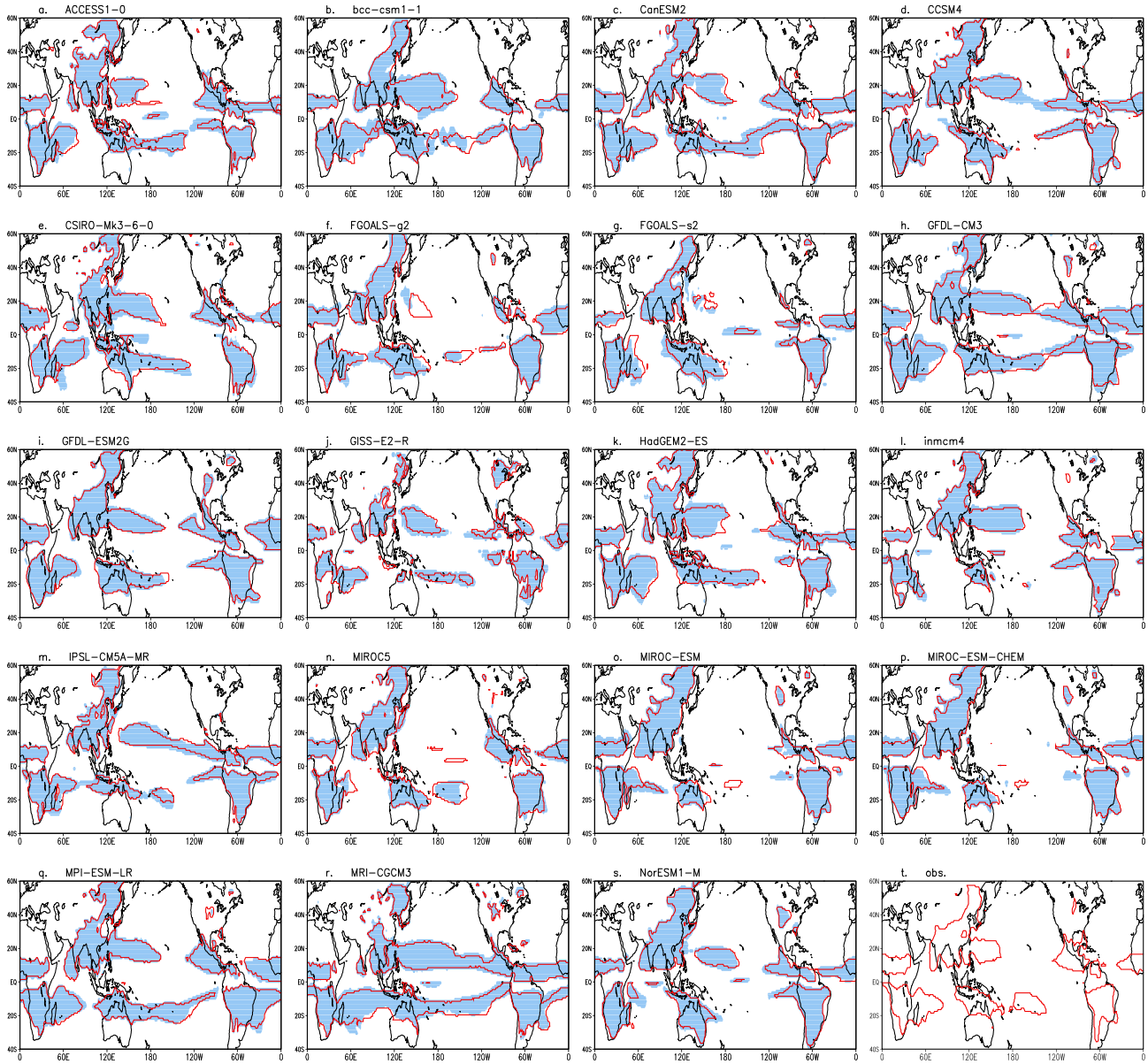

Figure 2. Simulated GMA derived from the historical (red contours) and RCP4.5 (blue shadings) outputs of individual CMIP5 CGCMs. The observed GMA is also shown in the fifth row of the fourth column.

Reconstructed Sea Surface Temperature (ERSST V3) [*Smith et al*., 2008]. The HadISST1 and ERSST monthly mean SST data have a horizontal resolution of 1° and 2°, respectively.

2.2. Methodology

[10] Precipitation is the most fundamental variable used to describe the monsoon climate, which is characterized by a wet summer and a dry winter. Following *Liu et al*. [2009], the global monsoon area (GMA) is defined as the regions where the annual range (i.e., the difference between local summer and winter) of precipitation exceeds 2 mm d^{-1}, and the local summer precipitation exceeds 55% of annual rainfall. In the Northern Hemisphere, the local summer is defined as May to September (MJJAS), and the local winter is defined as November to March (NDJFM); in the Southern Hemisphere, the definition is just the opposite. Considering the effect of climatology rainfall biases associated with different models on the GMA definition, and the possible changes in the annual rainfall cycle under global warming, we conducted a sensitivity test using various criteria for the annual range of rainfall (e.g., 1.5, 2, 2.5, and 3 mm d^{-1}) and summer-to-annual rainfall ratios (e.g., 45%, 50%, 55%, 60%, and 65%) to derive the GMA. It is found that the change rates of the GMA associated with a warming climate are not sensitive to these ratios. The GMP is defined as the mean of summer rainfall in the monsoon area. As the actual area of each grid changes with latitude, an area-weighting metric was used to calculate the GMA and GMP. A global monsoon intensity (GMI) index is defined to measure the global monsoon precipitation amount per unit area [*Hsu et al*., 2011]. The three global monsoon indices are derived from the climatology monthly rainfall for the periods

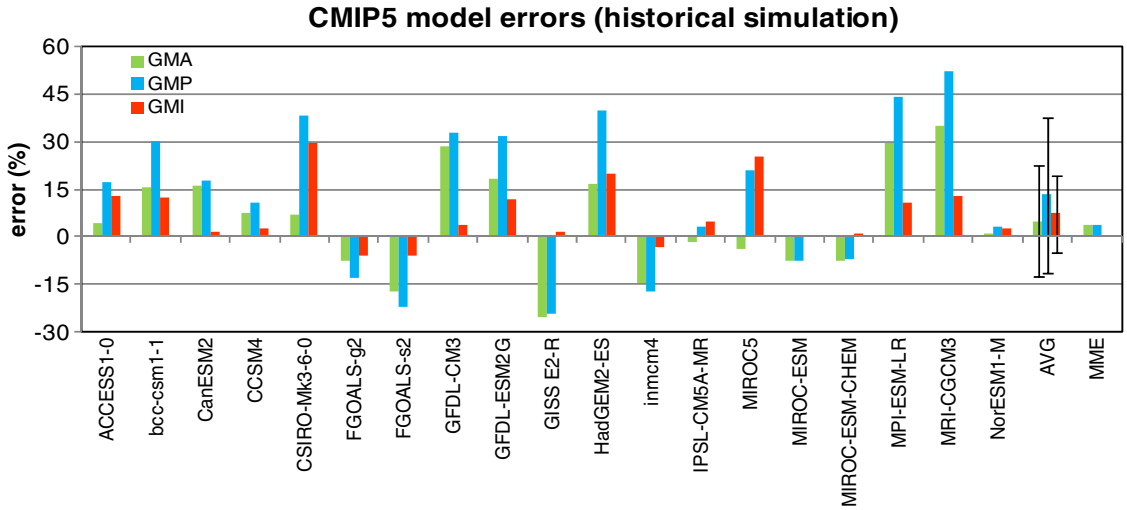

Figure 3. Simulation biases of GMA (green), GMP (blue), and GMI (red) relative to observations [i.e., $(X_{model} - X_{obs.})/X_{obs.}$] of the 19 individual CMIP5 models. Bars with whiskers indicate 19-model averages and inter-model standard deviations. The results derived from MME mean precipitation are revealed in the rightmost bars. Observed GMA, GMP, and GMI are 8.25×10^7 km^2, 5.67×10^{11} m^3 d^{-1}, and 6.86 mm d^{-1}, respectively.

1979–2003 and 2075–2099 to illustrate the characteristics of the present-day and future global monsoons, respectively.

[11] To analyze the interannual variability of monsoon rainfall and its relationship with ENSO, we examine the variations of GMP and ENSO in a typical monsoon year [*Yasunari*, 1991] rather than the calendar year. The GMP includes rainfall in both the boreal (JJA) and austral summers (DJF) through the two successive calendar years. Similarly, the evolution of ENSO extremes generally spans two calendar years, with a developing phase during the early boreal summer, a mature phase toward the end of the calendar year, and a decaying stage in the succeeding boreal spring. Thus, a monsoon year defined as the year between May and the following April, is the most appropriate time frame over which to describe the interannual variability of GMP, ENSO, and their relationship with each other [*Wang et al.*, 2011].

3. Climatology Global Monsoon Activity in the Historical Simulations

[12] Figure 1 shows the spatial distributions of climatology annual mean precipitation, the annual range of precipitation, and the GMA derived from observational data and MME mean precipitation from the 19 CMIP5 models. The MME annual mean precipitation field agrees well with the observations, with a pattern correlation coefficient of 0.9 (Figures 1a and 1d). The models capture the heavy rainfall regions along the ITCZ, the South Pacific convergence zone (SPCZ), the Indo-Pacific warm pool, and the midlatitude storm tracks. However, precipitation in the Pacific ITCZ and SPCZ is slightly overestimated.

[13] The monsoon climate features a large contrast between the wet and dry seasons. We further assess the capability of the models to simulate the annual range of rainfall (Figure 1e) and associated GMA (Figure 1f). The simulated patterns of the annual range of precipitation and the GMA resemble the observations (Figures 1b and 1c). Six distinct monsoons, including the Asian, Australian, North American, South American, West African, and South African monsoons, are clearly produced by the MME mean precipitation in the CMIP5 historical simulations. Some biases of extended monsoon domain are found over the Pacific and Atlantic sectors (Figure 1f), where the annual range of precipitation is overestimated by the models (Figure 1e).

[14] The ability of individual CMIP5 models to simulate the GMA pattern, total monsoon rainfall amounts, and monsoon intensity are presented in detail in Figures 2 and 3. Most of the CMIP5 models reproduce the major monsoon regions reasonably well. The FGOALS and MIROC model families (GISS-E2-R and INMCM4) do not generate the western Pacific monsoon (Australian monsoon), and thus they tend to underestimate the GMA (Figures 2 and 3). In contrast, some models (GFDL-CM3, MPI-ESM-LR, and MRI-CGCM3) significantly overestimate the GMA (Figure 3), in particular in the oceanic monsoon area (Figure 2). These GMA biases may affect the accuracy of the model's GMP estimations because more (less) monsoon rainfall would be measured within a larger (smaller) monsoon domain. As a result, models that overestimate (underestimate) the GMA generally overestimate (underestimate) the GMP. The bias is improved in the GMI, which is based on the rainfall amount per unit area. The inter-model standard deviation (or uncertainty) of simulated GMI is smaller than GMA and GMP. We note that, despite large variations in individual model performance, the GMA, GMP, and GMI derived from the MME mean precipitation show surprisingly good agreement with the observations (Figure 3).

4. Global Monsoon Changes Projected by the RCP4.5 Simulations

4.1. Changes in GMA, GMP, and GMI

[15] The projected change in the GMA derived from the MME mean precipitation in the CMIP5 models is shown in Figure 4a. The GMA patterns projected by individual models are shown in Figure 2. The MME result shows that the GMA tends to expand along the edges of present-day

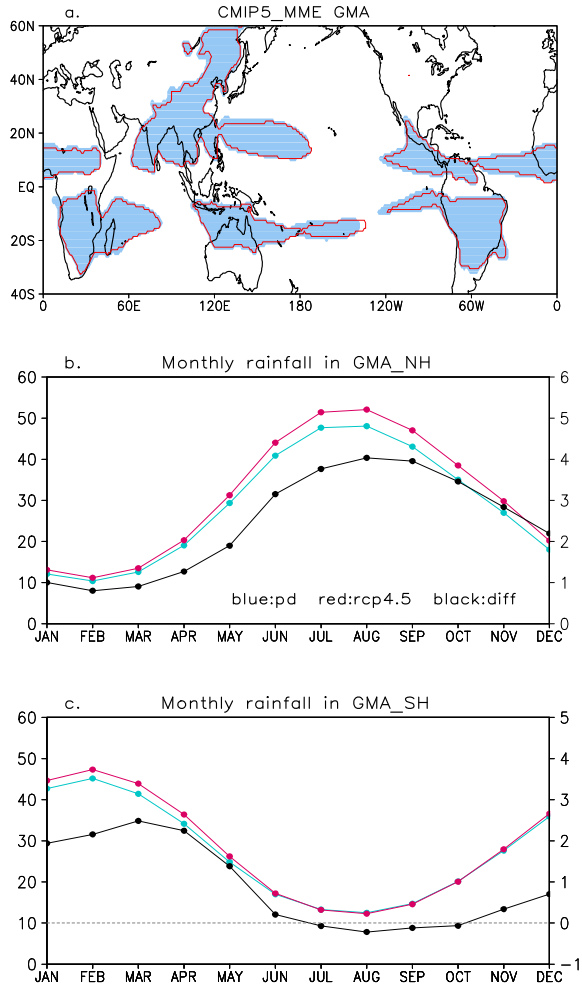

Figure 4. (a) As in Figure 2 except for the GMA derived based on the MME mean precipitation fields. (b) MME mean monthly rainfall variations within the northern hemispheric monsoon regions in the historical simulations (blue), RCP4.5 projections (red), and their difference (black). Units are 10^3 mm d^{-1} on the left axis for the historical and RCP4.5 runs, but their difference is on the right axis. (c) As in Figure 4b except for the rainfall within the southern hemispheric monsoon regions.

GMA under global warming. Very small areas with a decreased GMA are projected. The dominant feature of an expanding GMA may arise from the enhancement of seasonal rainfall cycles under global warming [*Chou and Lan*, 2012]. Figures 4b and 4c illustrate the monthly rainfall variations within the GMA in the Northern and Southern Hemispheres, respectively. In terms of an absolute change to the rainfall amount, a prominent increase in summer monsoon rainfall is projected over the globe. However, winter monsoon rainfall shows less significant changes, with a small increase (decrease) in the northern (southern) monsoon area. Note that, from the percent change point of view, the increase of northern winter monsoon rainfall is comparable to that of northern summer monsoon rainfall. The results suggest that global warming may induce a wetter summer over the global monsoon regions, and enlarge the contrast between rainy and dry seasons (especially in the southern monsoon area).

[16] To derive a quantitative measure of GMA change, we calculate the rate of change between the historical and RCP4.5 simulations from each CMIP5 model, as well as the changes in the GMA derived from the MME mean precipitation under the two scenarios. Comparing GMA change rates with increasing global mean surface air temperature (Figure 5a) provides an indication of whether the amplitude of GMA change is modulated by the extent of global warming. It is well known that global warming is a robust climate change signal [*IPCC*, 2007], while the temperature increase from the late 20th century to the late 21st century shows a wide range (1–3 K) among the CMIP5 projections.

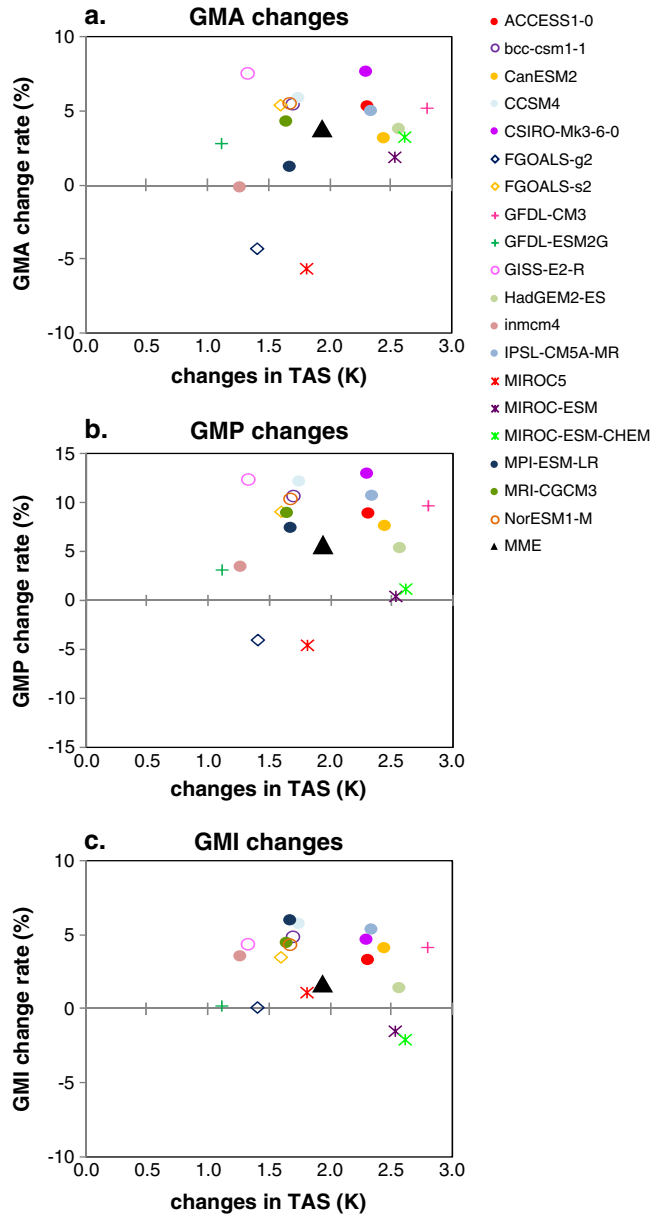

Figure 5. Changes in globally averaged surface air temperature (K) versus change rates (%) of (a) GMA, (b) GMP, and (c) GMI between the RCP4.5 (2075–2099) and historical (1979–2003) simulations from the 19 individual CMIP5 models, and the results based on MME mean precipitation and temperature (black triangles).

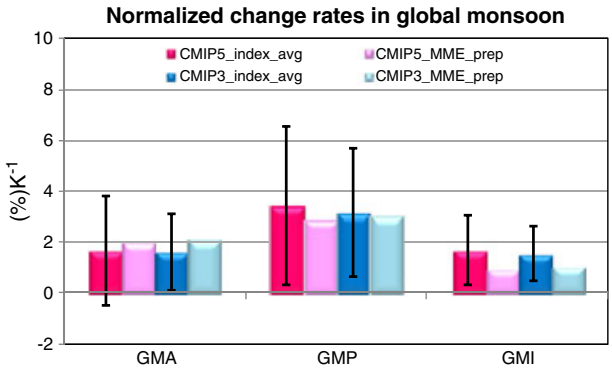

Figure 6. Averages and inter-model standard deviations (red bars with whiskers) of GMA, GMP, and GMI change rates between RCP4.5 and historical simulations in the 19 CMIP5 models. Pink bars show the change rates calculated from the CMIP5 MME mean precipitation. The global monsoon change rates are normalized by the globally averaged surface air temperature changes (% K^{-1}). Dark and light blue bars are reproduced from *Hsu et al.* [2012] for the change rates of GMA, GMP, and GMI between A1B (2075–2099) and 20C3M (1979–2003) in 24 CMIP3 models.

Similarly, the increased GMA is robust in the CMIP5 models (with the exception of MIROC5 and FGOALS-g2), but with various rates of increase ranging from 1% to 10%. The change rate of the GMA derived from the MME rainfall is around 3.9% (marked by a black triangle in Figure 5a). The increase in the GMA is significant (exceeding 95% significance level) in 14 of the 17 models and the MME result. It is noted that the increasing rates of GMA change do not significantly correlate with the increases in global mean air temperature. The correlation coefficient between GMA change rates and the air temperature anomaly projected by the 19 CMIP5 models is around 0.25 (Figure 5a).

[17] The expansion of the GMA may make a large contribution to changes in GMP, as a larger monsoon region would probably receive more rainfall. As shown in Figure 5b, enhanced GMP is projected consistently by the CMIP5 models except for MIROC5 and FGOALS-g2, which predict a reduced GMA. The enhancement of GMP is statistically significant in 15 of the 17 models. The MME mean precipitation indicates a 5.7% increase in GMP, which exceeds the 95% significance level. Because the rate of increase in GMP is generally larger than the rate of increase in GMA, the GMI index (rainfall change per unit area) shows an increase of 1% to 6% in 17 of 19 CMIP5 projections. The enhanced GMI is significant at the 95% confidence level in 14 of the 17 models. The decreased GMI in two of the models (MIROC-ESM and MIROC-ESM-CHEM) is due to smaller increases in GMP than GMA (Figure 5c). No significant linkage is found between an increase in global mean air temperature and the GMP/GMI change rates.

[18] The projected changes in GMA, GMP, and GMI are summarized in Figure 6, which shows the average change rate from the 19 models (red bars), with the inter-model standard deviations (whiskers denote one standard deviation), and the change rates calculated based on the CMIP5 MME mean precipitation in the present-day and global warming simulations (pink bars). Considering the various extents of global warming projected by the CMIP5 models (Figure 5), here we show the global monsoon changes normalized by the global mean surface warming. The increasing rate of GMP (GMA and GMI) is around 3–4% (1–2%) when the global surface air temperature increases by 1 K (Figure 6). As a large population lives within the land monsoon regions, the relative contributions of global monsoon changes over the land and ocean are further examined (Table 2). The results show that the increasing rates of GMA and GMP over oceanic regions are about twice as large as that over land. The GMI shows a comparable intensification over global land and oceanic monsoon areas.

[19] The CMIP5 models generally have a higher resolution and improved model physics relative to the earlier CMIP3 models. To gauge whether there is any difference between the two generations of CMIP coupled models, the change rates of the GMA, GMP, and GMI based on 24 CMIP3 model projections [reproduced from *Hsu et al.*, 2012] are shown in Figure 6 for comparison. While the range of the 19 CMIP5 simulations seems slightly larger than that generated by the 24 CMIP3 simulations, no significant differences are evident between the CMIP5 and CMIP3 models regarding the increases in the GMA, GMP, and GMI in response to global warming. The similarity of projected changes to the global monsoon in the CMIP3 and CMIP5 models suggests that the enhanced GMA, GMP, and GMI represents a robust signal across the different physical packages of these coupled models.

4.2. Moisture Diagnoses of GMP Change

[20] To develop a better understanding of the physical processes that cause the increase in GMP, we examine a column-integrated moisture budget within the GMA from both the present-day and future warming simulations. The GMP changes may be attributed to changes in horizontal moisture advection, moisture convergence associated with vertical motion, and surface evaporation, as shown in the following equation:

$$\Delta \mathrm{GMP} = -\Delta\langle \mathbf{V} \cdot \nabla q \rangle - \Delta\langle q \nabla \cdot \mathbf{V} \rangle + \Delta \mathrm{E} \qquad (1)$$

[21] where **V** is the horizontal vector wind, q is the specific humidity, E is evaporation, $\langle\ \rangle$ indicates a vertical

Table 2. Change Rates (%) of Land and Oceanic GMA, GMP, and GMI Between the Historical and RCP4.5 Simulations[a]

	GMA		GMP		GMI	
Change Rate (%)	Land	Ocean	Land	Ocean	Land	Ocean
19-model avg. (inter-model STD)	1.89 (±3.11)	3.85 (±8.27)	4.45 (±4.11)	7.67 (±10.81)	2.52 (±2.11)	3.17 (±3.51)
MME rainfall	2.93	6.7	4.56	9.62	2.11	2.8

[a][i.e., $(X_{RCP4.5} - X_{historical})/X_{historical}$]. Upper panel indicates the averages and inter-model standard deviations of global monsoon change rates derived from the 19 individual models. Bottom panel presents the change rates calculated from the MME mean precipitation.

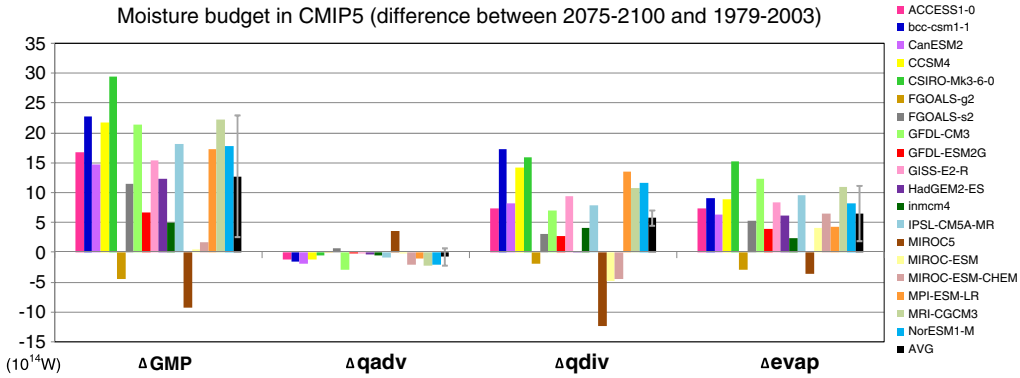

Figure 7. Moisture processes responsible for the GMP change in the 19 CMIP5 models. Changes in GMP, horizontal moisture advection, moisture convergence, and surface evaporation within the GMA (from left to right). Averages and inter-model standard deviations of the 19-model simulations are represented by black bars with whiskers (units 10^{14} W).

integration from 1000 to 100 hPa, ∇ is the horizontal gradient operator, and the operator $\Delta()$ represents the difference between global warming and present-day simulations (RCP4.5 minus historical simulations).

[22] The possible causes of changes in GMP in the individual CMIP5 models are shown in Figure 7. Overall, the enhanced GMP can be attributed to the increases in both the moisture convergence and surface evaporation under global warming. However, horizontal moisture advection makes an insignificant contribution to the increased GMP. Two models (FGOALS-g2 and MIROC5) with a decreased GMP show opposite moisture processes. The 19-model averaged result (black bars) indicates that the increased moisture convergence and surface evaporation make comparable contributions to the increased GMP.

[23] As changes in moisture and circulation both affect the changes in moisture convergence and evaporation, we further examine their relative contributions. As shown in equation (2) below, the difference of the moisture convergence term can be attributed to the difference of moisture convergence between present-day and future climate over the overlapping regions of present-day and future GMA plus the difference between the future moisture convergence over the GMA extension regions and the present-day moisture convergence over the GMA reduction regions.

$$-\Delta\langle q\times D\rangle = -\left(\sum_{A_{11}}\langle q_{gw}\times D_{gw}-q_{pd}\times D_{pd}\rangle + \sum_{A_{01}}\langle q_{gw}\times D_{gw}\rangle - \sum_{A_{10}}\langle q_{pd}\times D_{pd}\rangle\right) \quad (2)$$

[24] Here, the D indicates the divergence, and subscripts pd and gw denote the present-day and global warming simulations respectively. A_{11} represents the overlapping regions of present-day and future GMA, A_{10} represents the regions that belong to present-day GMA but not future GMA, and A_{01} denotes the regions that belong to future GMA but not present-day GMA. Because of relatively small areas of A_{10} and A_{01}, compared to the overlapping GMA area, we assume a uniform moisture field within A_{10} and A_{01}. Thus, the moisture convergence change term may be further decomposed into contributions from the dynamic process (ΔDY), the thermodynamic process (ΔTH) and the nonlinear process (ΔNL), as below.

$$\begin{aligned}-\Delta\langle q\times D\rangle &= -\left(\sum_{A_{11}}\langle q_{gw}\times D_{gw}-q_{pd}\times D_{pd}\rangle + \left\langle \overline{q_{gw}}^{A_{01}}\times\sum_{A_{01}}D_{gw}\right\rangle - \left\langle \overline{q_{pd}}^{A_{10}}\times\sum_{A_{10}}D_{pd}\right\rangle\right)\\ &= \Delta\mathrm{DY}+\Delta\mathrm{TH}+\Delta\mathrm{NL}\end{aligned}$$

$$\Delta\mathrm{DY} = -\left(\sum_{A_{11}}\langle q_{pd}\times(D_{gw}-D_{pd})\rangle + \left\langle \overline{q_{pd}}^{A_{10}}\times\left(\sum_{A_{01}}D_{gw}-\sum_{A_{10}}D_{pd}\right)\right\rangle\right)$$

$$\Delta\mathrm{TH} = -\left(\sum_{A_{11}}\langle(q_{gw}-q_{pd})\times D_{pd}\rangle + \left\langle(\overline{q_{gw}}^{A_{01}}-\overline{q_{pd}}^{A_{10}})\times\sum_{A_{10}}D_{pd}\right\rangle\right)$$

$$\Delta\mathrm{NL} = -\left(\sum_{A_{11}}\langle(q_{gw}-q_{pd})\times(D_{gw}-D_{pd})\rangle + \left\langle(\overline{q_{gw}}^{A_{01}}-\overline{q_{pd}}^{A_{10}})\times\left(\sum_{A_{01}}D_{gw}-\sum_{A_{10}}D_{pd}\right)\right\rangle\right) \quad (3)$$

[25] In equation (3), the over bar with A_{01} (A_{10}) indicates the area average over A_{01} (A_{10}). ΔDY is the part of GMP change associated with circulation change. ΔTH is the part of GMP change related to the water vapor change. ΔNL arises from the co-variation of circulation and water vapor changes.

[26] A similar approach was applied to the surface evaporation term. The change of surface evaporation may be expressed as

$$\Delta E = L\rho C_E\left(\sum_{A_{11}}\left[W_{gw}\times(q_s-q_a)_{gw}-W_{pd}\times(q_s-q_a)_{pd}\right] + \sum_{A_{01}}\left[W_{gw}\times(q_s-q_a)_{gw}\right]-\sum_{A_{10}}\left[W_{pd}\times(q_s-q_a)_{pd}\right]\right) \quad (4)$$

[27] where L is the latent heat, ρ is the air density at standard sea-level, C_E is the exchange coefficient, W is the surface wind speed, and q_s and q_a are the specific humidity at the sea surface and at 10 m, respectively. The total evaporation difference term may be decomposed into three parts:

$$\begin{aligned}
\Delta E &= L\rho C_E\left(\sum_{A_{11}}\left[W_{gw}\times(q_s-q_a)_{gw}-W_{pd}\times(q_s-q_a)_{pd}\right]\right.\\
&\quad\left.+\overline{(q_s-q_a)_{gw}}^{A_{01}}\times\sum_{A_{01}}W_{gw}-\overline{(q_s-q_a)_{pd}}^{A_{10}}\times\sum_{A_{10}}W_{pd}\right)\\
&= \Delta\mathrm{DY}+\Delta\mathrm{TH}+\Delta\mathrm{NL}\\
\Delta\mathrm{DY} &= L\rho C_E\left(\sum_{A_{11}}\left[(W_{gw}-W_{pd})\times(q_s-q_a)_{pd}\right]\right.\\
&\quad\left.+\left(\sum_{A_{01}}W_{gw}-\sum_{A_{10}}W_{pd}\right)\times\overline{(q_s-q_a)_{pd}}^{A_{10}}\right)\\
\Delta\mathrm{TH} &= L\rho C_E\left(\sum_{A_{11}}\left\{W_{pd}\times\left[(q_s-q_a)_{gw}-(q_s-q_a)_{pd}\right]\right\}\right.\\
&\quad\left.+\sum_{A_{10}}W_{pd}\times\left[\overline{(q_s-q_a)_{gw}}^{A_{01}}-\overline{(q_s-q_a)_{pd}}^{A_{10}}\right]\right)\\
\Delta\mathrm{NL} &= L\rho C_E\left(\sum_{A_{11}}\left\{(W_{gw}-W_{pd})\times\left[(q_s-q_a)_{gw}-(q_s-q_a)_{pd}\right]\right\}\right.\\
&\quad\left.+\left(\sum_{A_{01}}W_{gw}-\sum_{A_{10}}W_{pd}\right)\times\left[\overline{(q_s-q_a)_{gw}}^{A_{01}}-\overline{(q_s-q_a)_{pd}}^{A_{10}}\right]\right)
\end{aligned}\tag{5}$$

[28] where the first term in the right-hand side (ΔDY) is attributed to changes in surface wind speed, the second term (ΔTH) is attributed to changes in sea-air specific humidity difference ($q_s - q_a$), and the third term (ΔNL) is attributed to the nonlinear process related to both the wind speed and the humidity difference changes.

[29] The contributions of dynamic, thermodynamic, and nonlinear processes to the changes in moisture convergence and evaporation are shown in Figure 8. A robust feature simulated by the CMIP5 models is that the thermodynamic effect due to increased water vapor content plays an important role in enhancing both the moisture convergence and evaporation. However, the dynamic effect is less consistent among models, and shows different contributions to moisture convergence (Figure 8a) and evaporation (Figure 8b). Most of the CMIP5 models (15 of 19) suggest a decrease in monsoon rainfall associated with a weaker monsoon convergence flow under global warming. Although the thermodynamic component is offset to a large extent by the dynamic component, it still dominates the increased GMP (Figure 8a). As for evaporation, the dynamic effect related to the increased surface wind speed reveals positive, but minor, contributions in numerous CMIP5 models and in the 19-model averaged result (Figure 8b). Global distributions of surface wind speed change (not shown) confirm the strengthening of wind speed over monsoon regions. A decrease in wind speed occurs over the tropical oceans. Consequently, the enhanced surface evaporation may be driven by both the thermodynamic and dynamic contributors. The nonlinear terms are negligible in all of the simulations. It is worth indicating that the

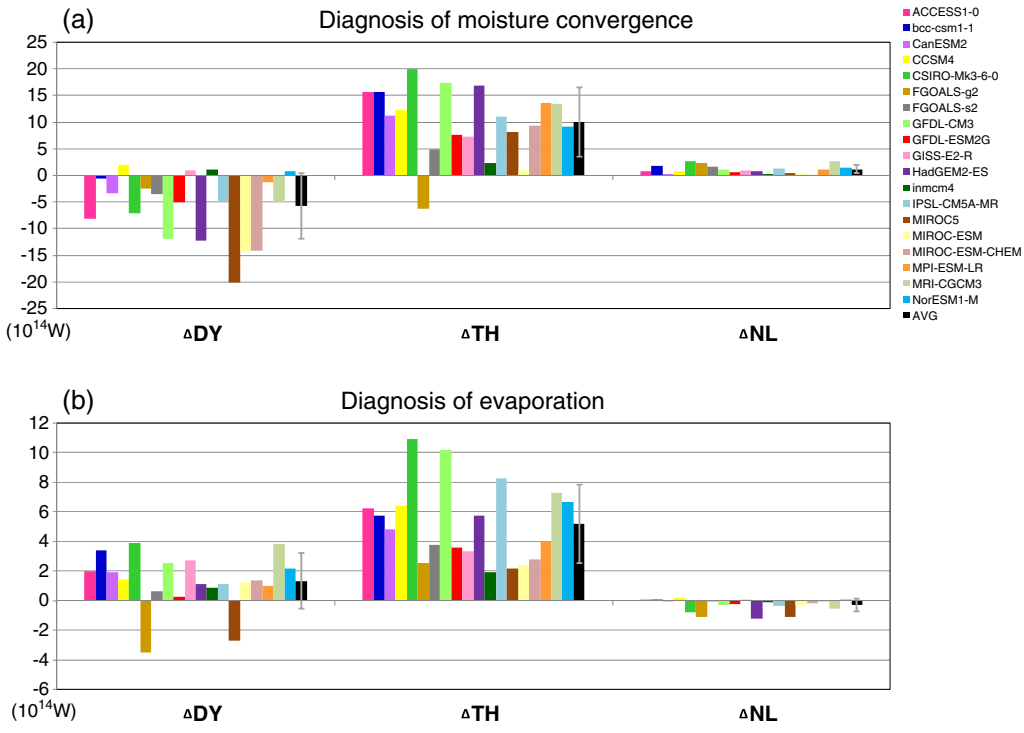

Figure 8. (a) Contributions of the changes in circulation, moisture, and the nonlinear product of the two changes (from left to right) to the moisture convergence change derived from the 19 CMIP5 models and the averages/inter-model standard deviations of all models. (b) As in Figure 8a but for the contributions of the surface wind speed change, the moisture change, and the nonlinear product of the two changes to the evaporation change (units 10^{14} W).

effects of surface wind speed on the GMP change here are different from the results projected by some high-resolution AGCMs [*Hsu et al.*, 2012]. Whether the global warming would induce a slowdown of tropical circulations remains uncertain [*Vecchi and Soden*, 2006; *Richter and Xie*, 2008; *Solomon and Newman*, 2012; *Meng et al.*, 2012].

5. Interannual Variability of Global Monsoon Precipitation

[30] To determine the intensity of the interannual variability of the present-day and future GMP, we calculate the interannual standard deviation of GMP over the 25 year periods 1979–2003 and 2075–2099, respectively (Figure 9a). While individual CMIP5 models simulate a wide range in the intensity of interannual variability in GMP, the average of models ($16.3 \times 10^9\,m^3\,d^{-1}$) is close to the observation ($18.8 \times 10^9\,m^3\,d^{-1}$). More than half of the simulations (12 of 19 models) show a strengthening of year-to-year GMP variation in the RCP4.5 projections. The average of the 19-model projection is $18.6 \times 10^9\,m^3\,d^{-1}$. This intensification of interannual variability in GMP is statistically significant at the 90% level (*t*-test). The changes in the interannual variability of the land and oceanic monsoon rainfall are further compared in Table 3. The amplitude of interannual variability of the oceanic monsoon rainfall is larger than that of the land monsoon rainfall in both the present-day and future climates. However, the stronger change in the year-to-year GMP rainfall comes from the land monsoon. The increase in the interannual standard deviation of land monsoon rainfall from historical ($8.3 \times 10^9\,m^3\,d^{-1}$) to RCP4.5 ($10.4 \times 10^9\,m^3\,d^{-1}$) simulations reaches a 95% significant level. This

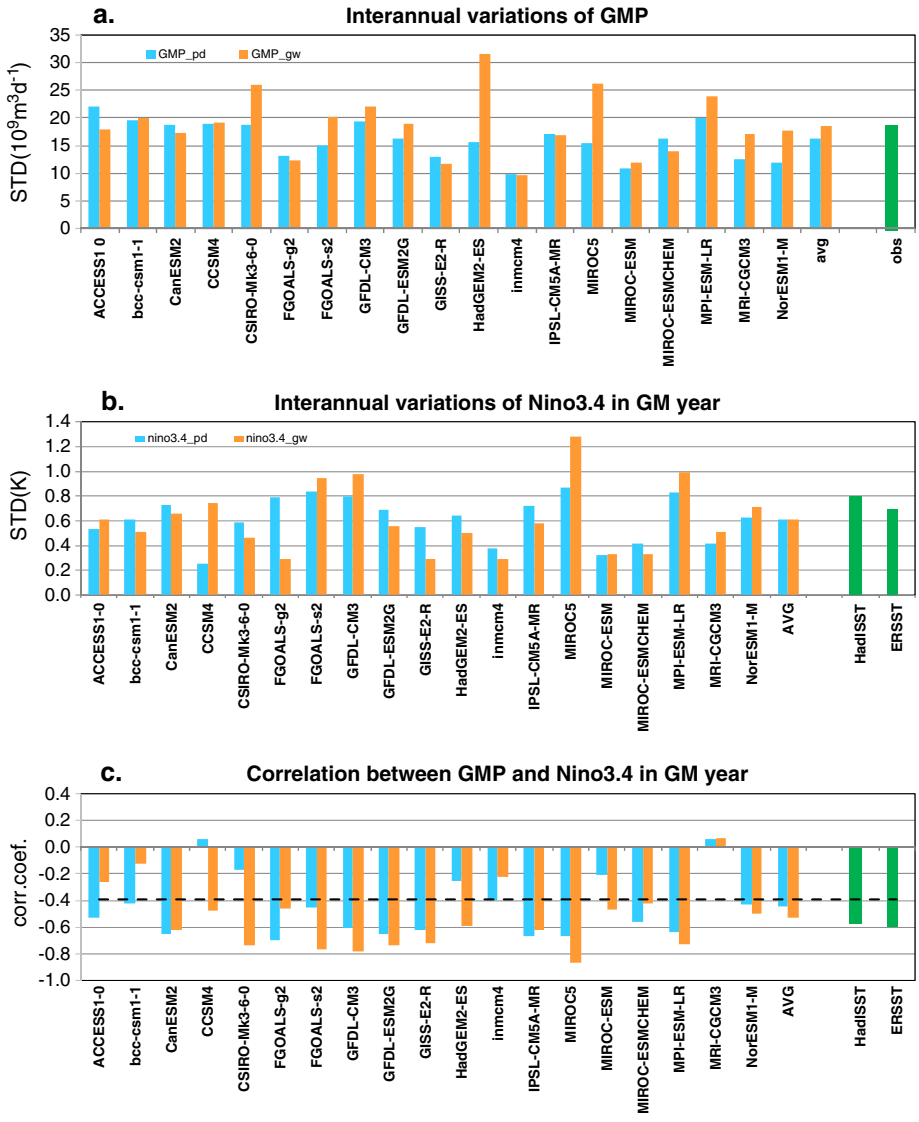

Figure 9. Standard deviations of simulated (a) GMP ($10^9\,m^3\,d^{-1}$) and (b) Niño3.4 SSTA averaged over the monsoon year (K) for 1979–2003 in the historical run (blue bars) and for 2075–2099 in the RCP4.5 run (orange bars) from the 19 CMIP5 models and the average values of all models. Observations (1979–2003) are shown by the green bars. (c) As in Figures 9a and 9b but for the correlation coefficients between GMP and Niño3.4 SSTA. Black dashed line denotes the 95% significance level.

Table 3. Strengths of Interannual Variability of GMP Over Land and Ocean Based on Observations (1979–2003), CMIP5 Historical Simulations (1979–2003), and RCP4.5 Projections (2075–2099), and the Correlation Coefficients Between GMP and Niño3.4 SSTA During the 25 year Periods[a]

	STD of 25 year GMP (unit: 10^9 m^3 d^{-1})			GMP-ENSO Correlation Coefficient	
Scenarios	Land	Ocean		Land	Ocean
Observation	9.2	12.9	HadISST	−0.65*	−0.38
			ERSST	−0.67*	−0.38
Historical	8.3	12.5		−0.46*	−0.29
RCP4.5	10.4	13.3		−0.57*	−0.29

[a]Correlation coefficients exceeding 95% confidence level are marked by asterisks.

suggests that more extreme wet and dry events may occur over global land monsoon regions as the climate warms [*Lu and Fu*, 2010; *Turner and Annamalai*, 2012].

[31] The El Niño-Southern Oscillation is considered to have been a crucial factor in modulating the year-to-year GMP variations over past decades [e.g., *Zhou et al*., 2008; *Wang et al*., 2011], so it is desirable to examine the projected changes in ENSO and their relationship with changes in the interannual variability of GMP. In contrast to the significant enhancement of GMP variations at the interannual time scale (Figure 9a and Table 3), the average interannual variability of the Niño3.4 SST anomaly (SSTA) from the 19 CMIP5 models indicates a stable, or slightly weaker, ENSO in the future projections relative to the present-day simulations (Figure 9b). This result is consistent with the findings of *Kim and Yu* [2012], who found a weaker intensity of the eastern Pacific ENSO in the RCP4.5 projections compared with that in the historical simulations. It is interesting to note that although ENSO intensity tends to weaken in the future projections, the general ENSO-GMP relationship remains significant, and even becomes stronger under global warming (Figure 9c and Table 3). In the present-day simulations, around 90% (17 of 19 CMIP5 models) of the models reproduce the negative correlation between GMP and ENSO seen in the observations [*Wang et al*., 2011]; while only two models (CCSM4 and MRI-CGCM3) produce positive correlation coefficients. The average correlation coefficient from the 19 models is −0.45, which exceeds the 95% significant level. Under the RCP4.5 scenario, the negative correlation between GMP and ENSO is consistently projected by the CMIP5 models (with the exception of MRI-CGCM3), and more than half show an intensification (Figure 9c). The 19-model averaged correlation coefficient is −0.53 in the RCP4.5 projection, which is larger than present-day result ($r = -0.45$). A further comparison of ENSO influence on monsoon rainfall over land and oceanic regions (Table 3) shows that ENSO forcing is significantly correlated with land monsoon rainfall in both observation and the historical simulations. This linkage is enhanced under global warming. In contrast, the correlation between ENSO events and oceanic monsoon rainfall is not statistically significant and shows no apparent changes under a warmer climatic regime (Table 3).

[32] To confirm the role of ENSO in modulating the interannual variability of GMP, we analyze the spatial distribution of the correlation coefficient between the GMP and global SST. The observed HadISST/ERSST anomalies and GMP are negatively correlated over the tropical central-eastern Pacific and Indian Ocean, but positively correlated in the western Pacific (Figures 10a and 10b). As in the observation, there is a well-defined relationship between GMP and local SST in the central-eastern Pacific shown in the average correlation map from the 19 CMIP5 historical simulations. The positive (negative) correlation is also found in the western Pacific (Indian Ocean), while it is less significant in the models (Figure 10c). This indicates the dominance of the ENSO signal in the interannual variability of GMP in the models. The future projected GMP-SST correlation pattern resembles the present-day simulations, and ENSO remains the most important oceanic forcing of the year-to-year GMP variations under global warming (Figure 10d). The analysis of the relationship between GMP and ENSO (Figures 9c and 10) suggests that the interannual variability of GMP may have potential predictability if the models can reasonably capture the fluctuation of the ENSO phase [*Zhou et al*., 2008].

[33] Many studies pointed out the obvious internal variability of interannual-to-decadal monsoon and ENSO variability [e.g., *Goswami*, 2006]. In order to assess the internal variability of the GMP-ENSO relationship, we analyze the correlations between the GMP and Niño3.4 SST in a 200 year segment of control simulations from the individual CMIP5 models. The results indicate that a negative correlation between the GMP and the ENSO is simulated consistently by the 19 CMIP5 models (Figure 11a). This is similar to the observation and historical run over a 25 year period (1979–2003). This suggests that the GMP-ENSO relationship obtained from the 25 year historical runs is not forced by external forcing, such as greenhouse gases and aerosols. In other words, the interannual-to-decadal variability of the GMP is largely due to internal processes of the atmosphere. In order to confirm the enhanced GMP-ENSO linkage associated with global warming (Figure 9c), we repeat the 25 year analysis using longer (50 year) data from both the present-day and future-warming simulations (Figure 11b). Consistent with the results of the 25 year analysis, the strengthening GMP-ENSO correlation is found in the average of the 19 CMIP5 projections.

6. Conclusions

[34] In contrast to previous monsoon studies that focused on changes at the regional scale, this study examined the variability of the global monsoon [*Trenberth et al*., 2000; *Wang and Ding*, 2006] under present-day (1979–2003) and future (2075–2099) climate states by analyzing the historical and RCP4.5 simulations of 19 CMIP5 models. An evaluation of the CMIP5 historical simulations shows that the

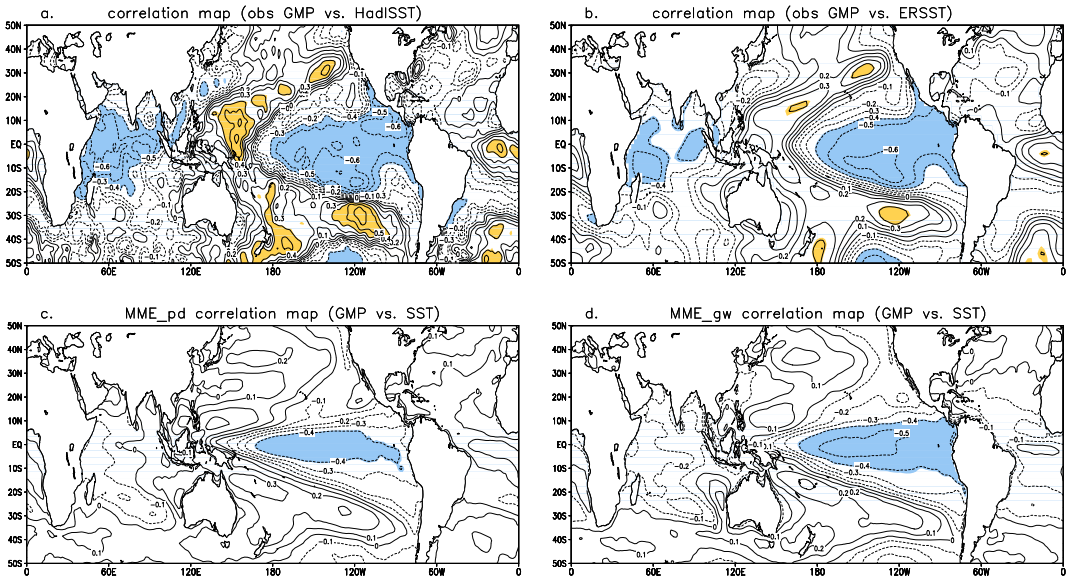

Figure 10. (a and b) Correlation patterns between observed GMP and SST anomalies averaged over the monsoon year for 1979–2003. The HadISST is used in Figure 10a while the ERSST is used in Figure 10b. (c and d) Same as Figures 10a and 10b but for the averages of correlation patterns from the 19 CMIP5 models under the historical (1979–2003) and RCP4.5 (2075–2099) scenarios, respectively. Areas exceeding 95% significant level are shaded.

GMA derived from the MME mean precipitation resembles the observations, with six distinct monsoon systems (Asian, Australian, North and South American, and West and South African monsoons) over the globe. The MME mean precipitation also produces accurate quantitative estimations of the GMA, GMP, and GMI, although the spread of individual model simulations is large.

[35] The GMA, GMP, and GMI all increase as the climate warms. The rates of increase of GMA, GMP, and GMI based on the CMIP5 simulations are around 1.9% K^{-1}, 3.2% K^{-1}, and 1.3% K^{-1}, respectively, and are surprisingly consistent with the CMIP3 results. This implies that the enhanced monsoon variability is a robust signal projected by these coupled models with different model physics, resolutions, and SST

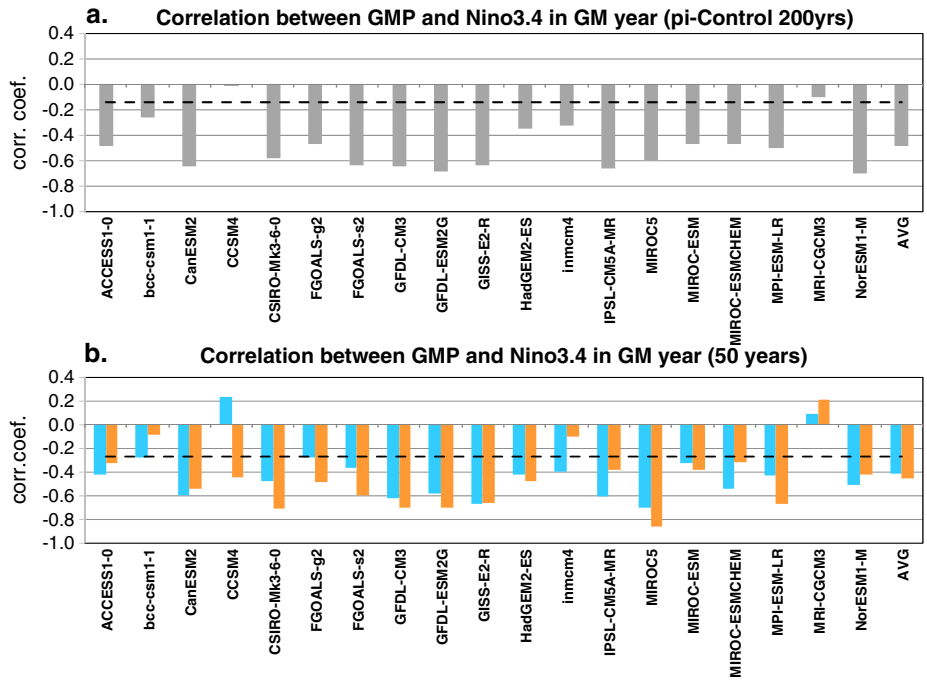

Figure 11. Same as Figure 9c but based on (a) 200 year data in the control simulations and (b) 50 year data in the historical run (1954–2003, blue bars) and RCP4.5 run (2050–2099, orange bars).

warming patterns [*Hsu et al*., 2012]. The expansion of the GMA is associated with the changes in the annual rainfall cycle in response to greenhouse gas warming forcing [*Chou and Lan*, 2012]. The CMIP5 models project a wetter summer, but little change to winter rainfall, over global monsoon regions, suggesting that global warming tends to induce an increase in the annual range of monsoon precipitation.

[36] To understand the physical processes responsible for the increased GMP, we examined the column-integrated moisture budget equation within the GMA. The results indicate that the increase in GMP is primarily caused by increases in moisture convergence and surface evaporation, whereas the effect of moisture advection is insignificant. Moisture convergence and surface evaporation include both the thermodynamic component associated with increased water vapor and the dynamic component related to changes in circulation. Further analysis indicates that the thermodynamic effect contributes positively to the moisture convergence, but is partly offset by the dynamic effect associated with a weakened monsoon circulation. The offsetting effect between the thermodynamic and dynamic components of the moisture convergence process was also seen in the modulation of regional monsoon rainfall changes [*Cherchi et al*., 2010; *Moise et al*., 2012]. Fewer studies have discussed the moisture processes related to surface evaporation change over monsoon regions. Our analysis shows that the enhanced surface evaporation within the GMA is primarily attributed to the increase in sea-air specific humidity difference. Changes to surface wind speed are a minor contributor to the increase in surface evaporation. The MME mean of the CMIP5 simulations shows a strengthening of wind speed in the global monsoon regions, but a reduction in wind speed over most of the tropical oceans.

[37] The CMIP5 models reproduce the amplitude of year-to-year GMP variability, and its negative correlation with ENSO found in observations [*Zhou et al*., 2008; *Wang et al*., 2011]. The average of the 19-model simulated correlation coefficients between GMP and Niño3.4 SSTA during a historical 25 year period (1979–2003) is −0.45, which is statistically significant at the 95% level. This GMP-ENSO relationship is also robust in the long (200 year) control integrations, suggesting that the interannual variability of GMP in the historical runs arises from processes internal to the coupled ocean-atmosphere system. Under global warming, the interannual variability of GMP is intensified, especially for rainfall variability over land monsoon regions. The relationship between GMP and ENSO also strengthens, with a correlation coefficient of −0.53 for the period 2075–2099. This suggests that the ENSO signal can be used as a potential predictor of the severe wet/dry global monsoon events under a future warmer climatic regime.

[38] **Acknowledgments.** Comments from three anonymous reviewers are greatly appreciated. This work was supported by NSF grant AGS-1106536, ONR grants N000141210450, and by the International Pacific Research Center that is sponsored by the Japan Agency for Marine-Earth Science and Technology (JAMSTEC), NASA, and NOAA. This is SOEST contribution xxxx and IPRC contribution xxx.

References

Adler, R. F., et al. (2003), The Version 2 Global Precipitation Climatology Project (GPCP) monthly precipitation analysis (1979–present), *J. Hydrometeorol.*, *4*, 1147–1167, doi:10.1175/1525-7541(2003)004<1147:TVGPCP>2.0.CO;2.

Annamalai, H., K. Hamilton, and K. R. Sperber (2007), South Asian summer monsoon and its relationship with ENSO in the IPCC AR4 simulations, *J. Clim.*, *20*, 1071–1092.

Cherchi, A., A. Alessandri, S. Masina, and A. Navarra (2011), Effects of increased CO_2 levels on monsoons, *Clim. Dyn.*, *37*, 83–101, doi:10.1007/s00382-010-0801-7.

Chou, C., and C.-W. Lan (2012), Changes in the annual range of precipitation under global warming, *J. Clim.*, *25*, 222–235, doi:10.1175/JCLID-11-00097.1.

Cook, K. H., and E. K. Vizy (2006), Coupled model simulations of the West African monsoon system: Twentieth- and twenty-first-century simulations, *J. Clim.*, *19*, 3681–3703, doi:http://dx.doi.org/10.1175/JCLI3814.1

Giorgi, F., P. H. Whetton, R. G. Jones, J. H. Christensen, L. O. Mearns, B. Hewitson, H. vonStorch, R. Francisco, and C. Jack (2001), Emerging patterns of simulated regional climatic changes for the 21st century due to anthropogenic forcings, *Geophys. Res. Lett.*, *28*(17), 3317–3320, doi:10.1029/2001GL013150.

Goswami B. N. (2005), The Asian monsoon: Interdecadal variability, The Asian Monsoon, edited by B. Wang, Praxis, Springer Berlin Heidelberg, 295–327 pp.

Hsu, P., T. Li, and B. Wang (2011), Trends in global monsoon area and precipitation over the past 30 years, *Geophys. Res. Lett.*, *38*, L08701, doi:10.1029/2011GL046893.

Hsu, P., T. Li, J.-J. Luo, H. Murakami, A. Kitoh, and M. Zhao (2012), Increase of global monsoon area and precipitation under global warming: A robust signal?, *Geophys. Res. Lett.*, *39*, L06701, doi:10.1029/2012GL051037.

Hsu, P., and T. Li (2012), Is "rich-get-richer" valid for Indian Ocean and Atlantic ITCZ?, *Geophys. Res. Lett.*, *39*, L13705, doi:10.1029/2012GL052399.

Hu, Z., M. Latif, E. Roeckner, and L. Bengtsson (2000), Intensified Asian summer monsoon and its variability in a coupled model forced by increasing greenhouse gas concentrations, *Geophys. Res. Lett.*, *27*(17), 2681–2684, doi:10.1029/ 2000GL011550.

Intergovernmental Panel on Climate Change (IPCC) (2007), Climate Change 2007: The Physical Science Basis. Contribution of Working Group I to the Fourth Assessment Report of the IPCC, edited by S. Solomon et al., Cambridge Univ. Press, Cambridge, U. K.

Kim, H.-J., K. Takata, B. Wang, M. Watanabe, M. Kimoto, T. Yokohata, and T. Yasunari (2011), Global monsoon, El Niño, and their interannual linkage simulated by MIROC5 and the CMIP3 CGCMs, *J. Clim.*, *24*, 5604–5618, doi:http://dx.doi.org/10.1175/2011JCLI4132.1

Kim, S. T., and J.-Y. Yu (2012), The two types of ENSO in CMIP5 models, *Geophys. Res. Lett.*, *39*, L11704, doi:10.1029/2012GL052006.

Kitoh, A., M. Hosaka, Y. Adachi, and K. Kamiguchi (2005), Future projections of precipitation characteristics in East Asia simulated by the MRI CGCM2, *Adv. Atmos. Sci.*, *22*, 467–478.

Li, W., R. Fu, and R. E. Dickinson (2006), Rainfall and its seasonality over the Amazon in the 21st century as assessed by the coupled models for the IPCC AR4, *J. Geophys. Res.*, *111*, D02111, doi:10.1029/2005JD006355.

Liu, J., B. Wang, Q. Ding, X. Kuang, W. Soon, and E. Zorita (2009), Centennial variations of the global monsoon precipitation in the last millennium: Results from ECHO-G model, *J. Clim.*, *22*, 2356–2371, doi:10.1175/2008JCLI2353.1.

Lu, R., and Y. Fu (2010), Intensification of East Asian summer rainfall interannual variability in the twenty-first century simulated by 12 CMIP3 coupled models, *J. Clim.*, *23*, 3316–3331, doi:http://dx.doi.org/10.1175/2009JCLI3130.1.

May, W. (2002), Simulated changes of the Indian summer monsoon under enhanced greenhouse gas conditions in a global timeslice experiment, *Geophys. Res. Lett.*, *29*, 1118, doi:10.1029/2001GL013808.

Meehl, G. A., and J. M. Arblaster (2003), Mechanisms for projected future changes in south Asian monsoon precipitation, *Clim. Dyn.*, *21*, 659–675, doi:10.1007/ s00382-003-0343-3

Meng, Q., M. Latif, W. Park, N. Keenlyside, V. Semenov, and T. Martin (2012), Twentieth century Walker Circulation change: Data analysis and model experiments, *Clim. Dyn.*, *38*, 1757–1773.

Moise, A. F., R. A. Colman, and J. R. Brown (2012), Behind uncertainties in projections of Australian tropical climate: Analysis of 19 CMIP3 models, *J. Geophys. Res.*, *117*, D10103, doi:10.1029/2011JD017365.

Rayner, N. A., D. E. Parker, C. K. Horton, C. K. Folland, L. V. Alexander, D. P. Rowell, E. C. Kent, and A. Kaplan (2003), Global analyses of sea surface temperature, sea ice and night marine air temperature since the late nineteenth century, *J. Geophys. Res.*, *108*(D14), 4407, doi:10.1029/2002JD002670.

Richter, I., and S.-P. Xie (2008), Muted precipitation increase in global warming simulations: A surface evaporation perspective, *J. Geophys. Res.*, *113*, D24118, doi:10.1029/2008JD010561.

Shongwe, M. E., G. J. van Oldenborgh, B. J. J. M. van den Hurk, B. de Boer, C. A. S. Coelho, and M. K. van Aalst (2009), Projected changes in mean and extreme precipitation in Africa under global warming.

Part I: Southern Africa, *J. Clim.*, *22*, 3819–3837. doi:http://dx.doi.org/10.1175/2009JCLI2317.1

Smith, T. M., R. W. Reynolds, T. C. Peterson, and J. Lawrimore (2008), Improvements to NOAA's historical merged land–ocean surface temperature analysis (1880–2006), *J. Clim.*, *21*, 2283–2296.

Solomon, A., and M. Newman (2012), Reconciling disparate twentieth-century Indo_Pacific ocean temperature trends in the instrumental record, *Nature Climate Change*, *2*, 691–699, doi 10.1038/nclimate159.

Taylor, K. E., R. J. Stouffer, and G. A. Meehl (2012), An overview of CMIP5 and the experimental design, *Bull. Am. Meteorol. Soc.*, *93*, 485–498, doi:10.1175/ BAMS-D-11-00094.1.

Trenberth, K. E., D. P. Stepaniak, and J. M. Caron (2000), The global monsoon as seen through the divergent atmospheric circulation, *J. Clim.*, *13*, 3969–3993, doi:10.1175/1520-0442(2000)013<3969:TGMAST>2.0.CO;2

Turner, A. G., and H. Annamalai (2012), Climate change and the South Asian summer monsoon, *Nature Climate Change*, online publication June 24, doi:10.1038/ NCLIMATE1495.

Ueda, H., A. Iwai, K. Kuwako, and M. E. Hori (2006), Impact of anthropogenic forcing on the Asian summer monsoon as simulated by eight GCMs, *Geophys. Res. Lett.*, *33*, L06703, doi:10.1029/2005GL025336.

Vecchi, G. A., and B. J. Soden (2007), Global warming and the weakening of the tropical circulation, *J. Clim.*, *20*, 4316–4340, doi:10.1175/JCLI4258.1.

Wang, B., and Q. Ding (2006), Changes in global monsoon precipitation over the past 56 years, *Geophys. Res. Lett.*, *33*, L06711, doi:10.1029/2005GL025347.

Wang, B., J. Liu, H.-J. Kim, P. J. Webster, S.-Y. Yim (2011), Recent change of the global monsoon precipitation (1979–2008), *Clim. Dyn.*, doi:10.1007/s00382-011-1266-z.

Webster, P. J. (1987), The elementary monsoon.Monsoons. Fein J. S. and Stephens P. L. (*Eds*), Wiley-Interscience, New York.

Xie, P. P., and P. A. Arkin (1997), Global precipitation: A 17-year monthly analysis based on gauge observations, satellite estimates, and numerical model outputs, *Bull. Am. Meteorol. Soc.*, *78*, 2539–2558, doi:10.1175/1520-0477(1997)078<2539:GPAYMA>2.0.CO;2.

Yasunari, T. (1991), The monsoon year—A new concept of the climatic year in the Tropics, *Bull. Amer. Meteor. Soc.*, *72*, 1331–1338, doi:http://dx.doi.org/10.1175/ 1520-0477(1991)072<1331:TMYNCO>2.0.CO;2

Zhou, T., R. Yu, H. Li, and B. Wang (2008), Ocean forcing to changes in global monsoon precipitation over the recent half-century, *J. Clim.*, *21*, 3833–3852, doi:10.1175/2008JCLI2067.1.